Effective Fuzzy Logic Control of a Stand-alone Photovoltaic Pumping System

M. Bahloul*‡, L. Chrifi-Alaoui**, M. Souissi*, M. Chaabane*, S. Drid***

* Laboratory Lab-STA, National Engineering School of Sfax, 3072, Tunisia.

** Laboratory LTI, University of Picardie Jules Verne, 02200, Cuffies, France.

*** Laboratory LSPIE, Laboratory University of Batna, 5000, Algeria.

‡Corresponding Author; M. Bahloul; email: eng.mohamed.bahloul@ieee.com

Received:24.03.2015 Accepted:10.04.2015

Abstract- This paper presents an effective control of a stand-alone batteryless photovoltaic (PV) pumping system. The whole design (configuration and control) is oriented in order to minimize the cost and maximize the effectiveness, the efficiency and the reliability of the whole system. Beyond the withdrawal of the battery and the rotor speed sensor, the system is composed only of a DC-DC boost converter, a DC-AC inverter, an Induction Motor (IM) and a centrifugal pump. In order to control the dc-link voltage and maximize the efficiency of the IM, a Fuzzy Logic Controller (FLC) is introduced. The validity and the effectiveness of the proposed FLC is tested and confirmed by a simulation under various climate changes.

Keywords - Photovoltaic pumping system, Induction Motor, Efficiency optimization, Fuzzy logic.

1. Introduction

The water access either for individual needs in a community, or for irrigation, presents one of the main factors for the development of remote area in developing countries. Since the connectivity to the national electric grid presents an expensive investment in such isolated area, the PV pumping system is one of the most economical and efficient ways [1]. Although this solution is applied and commercialized since the last decade, it is still taking a considerable focus in order to reduce the cost and to improve its efficiency, effectiveness and robustness [1, 2].

The use of electrical motor is the most popular solution to convert the electrical energy generated by the PV Generator PVG to a mechanical energy used to train pumps. The use of DC motors was incorporated with the first generation of PV pumping system. In such configuration, the direct connection between PVG and the motor is the main advantage [3]. However, the maintenance issue remains the major drawback. With the development of power electronics, the use of AC Motors was widely deployed. Nevertheless a DC/AC inverter has to be added to the installation. Comparing to the synchronous motor, the IM presents an attractive and competitive technical choice in such application thanks to its low cost and its performances in terms of reliability, rigidness and robustness [4, 5].

Taking into consideration the high investment on the PV pumping system, an imperative consideration of the optimization of the end to end system have to be taken. Thus, several optimization strategies and algorithms were developed to maximize the ratio of pumped water to generated energy. These methods focus on the efficiency maximization of the PVG or/and the motor. Then, the whole system efficiency is evaluated. Considering the PVG, many approaches of Maximum Power Point Tracking (MPPT) algorithms have been developed such as 1) fractional open circuit voltage algorithms, 2) fractional short circuit current algorithms, 3) Perturb And Observe algorithms (P&O), 4) INcremental Conductance algorithms (INC), 5) artificial-intelligence-based algorithms [6,7,8]. Moreover, from motor point of view, the main aim is to supply a maximum mechanical output power with a minimum delivered electrical input. This objective could be achieved while applying an efficient control strategy. Indeed, the motor efficiency can be optimized by the control of dc-link voltage [9] and/or the level of the motor magnetic flux [9]. The latest one is well known as field weakening method allowing the minimization of power losses when the motor runs at a low speed with a partial load. In addition, the field-oriented control (FOC) presents an attractive method that enhances the performances of IM comparing to the conventional scalar v/f one [10,11]. It is worth noting that speed information is a mandatory requirement to achieve the FOC implementation [12,13]. However, the mechanical speed sensors are associated with several drawbacks. Indeed, it increases the size and cost of the drive system. In addition it reduces the robustness and reliability (regular maintenance of the speed sensor). Furthermore, the use of speed sensor for pumping applications, especially in remote area, is not appropriate due to environmental constraints. Accordingly, a considerable attention should be paid to remove the encoder without impacting the performance of the control system.

The PV pumping systems using AC motors were generally accompanied by an energy system storage. We

note that PV pumping systems with a lead acid battery were the subject of many studies [14]. This storage system improves the efficiency of the water pump. In addition, it enhances the stability of the global system while decoupling the dynamics the PVG and the IM. Indeed, through a bidirectional DC-DC converter, the energy balance between the PVG, the battery and the motor is ensured. Furthermore, a constant dc-link peak voltage is guaranteed. However, the use of battery bank implies a lot of drawbacks: 1) an additional installation expensive cost, 2) an additional maintenance effort and cost, 3) a decrease of the overall system lifetime, 4) an environmental impact. These drawbacks have to be considered especially for remote area in developing countries were individual incomes is too low and government and public investment are too limited.

Obviating the requirement to overcome these limits, a batteryless PV pumping system was developed and some configurations were adopted. The energy optimization and the efficiency consideration were the main challenges. In Corrêa et al. [15], an optimized configuration of a batteryless PV pumping system is presented. An MPPT control of the PVG and a minimum operation loss of the IM are taken into consideration. The IM is controlled via an v/f strategy. In Betka and Attali [4], and on the basis of the optimal control theory, interesting results on the motor efficiency improvement are presented. In addition, field-oriented and MPPT controls were considered. The dc-link voltage is also controlled via a PI action. The authors in Vitorino et al. [9] have employed a push-pull converter downstream of the PVG. In addition, an open loop sensorless vector control strategy is used. The efficiency of the IM is enhanced via optimal dc-link voltage and field weakening controls. In Cararcas et al. [16], the authors focused on the design of a DC-DC converter more suitable to drive the three phases IM in case of batteryless application. A v/f IM control strategy is employed and an efficiency operation is considered via an optimal control of the dc-link voltage.

The purpose of the actual study is to design an FLC controller that ensures both the control of dc-link voltage and optimization of IM efficiency. The dc-link voltage is controlled through an energy balance between the PVG, the IM and the capacitor of the dc-bus. The control objective consists on maintaining the dc-bus voltage constant following any change of the transited power. The IM efficiency is improved by a fuzzy control of the reference flux level in case of sensorless Indirect Rotor Field Oriented Control (IRFOC) strategy.

2. System description

The figure1 shows the proposed configuration of the stand-alone pumping system. As mentioned in the introduction, the design is driven to present the most economic and effective solutions. Indeed, we propose a conventional MPPT to maximize PVG power generation through the control of the duty cycle of a boost DC-DC converter. The DC-DC converter output is linked directly to the DC-AC inverter via a dc-link capacitor. The drivers of the inverter are supplied via a reference PWM signals generated by a sensorless IRFOC algorithm. A centrifugal pump is linked to the shaft of the IM and characterized by a load torque proportional to the square of the speed on the rotor shaft.

We note that the global system starts whenever a minimum solar radiation of 100 W/m^2 is detected. Based on this level, a minimum rotor speed on the shaft of the IM will be ensured. Consequently, the centrifugal pump can start to pump water.

The first main advantage is to maintain the voltage in the dc-bus voltage constant regardless to the climate change. We note that since a conventional boost DC / DC converter is used in the proposed configuration of the pumping system, it is more judicious to fix the value of the dc-link voltage to ensure a better system stability and a decoupling between the dynamics of the IM and the PVG. This control is ensured especially by an adequate computing of the reference rotor speed (which consists of the first FLC output). While the dc-bus voltage is under the reference value (600v), the FLC controls the IM and the pump to compensate a less energy than the available one on the dc-bus input (and vice versa while the dc-bus voltage is over the reference). The whole available energy is consumed by the pump while the dc-bus voltage is about to reach the reference.

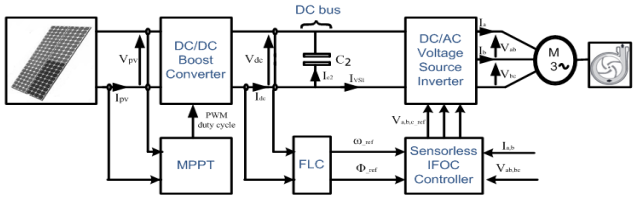

Figure 1: Batteryless PV pumping system.

The second main advantage of this configuration is the energy saving. Indeed, three levels of optimization are considered. The first one is based on a conventional MPPT control of the PVG. The sensorless IRFOC presents the second level. The last level is so called the field weakening operation. Indeed, the proposed FLC ensures the variation of the reference flux on the sensorless IRFOC in order to improve the motor efficiency.

2.1. PVG model

In the literature, many models of the PV cell have been developed to deal with its high nonlinear dynamic. We can distinguish single, double or three-diode model. In this study, we will consider the single-diode model due to its simplicity and its effective use in simulation [17]. This model can be presented by the electrical equivalent circuit described in the Figure 2. It consists of a current generator in parallel with a diode, an internal parallel and series resistor respectively named $R_{s,cell}$ and $R_{p,cell}$.

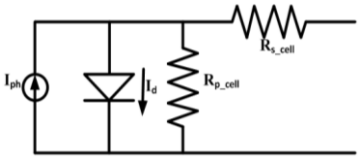

Figure 2: PV cell model with single diode.

In the practice, commercialized solar modules are formed generally by a number of cells assembled in parallel Np or /and in series Ns. In addition, a datasheet is provided and includes the main following information about the product (Table I).

Table I: Data sheet information of a PV panel.

The nominal open-circuit voltage	$V_{oc,n}$
The nominal short-circuit current	$I_{sc,n}$
The voltage at the MPP	V_{mp}
The current at the MPP	I_{mp}
The open-circuit voltage/temperature coefficient	K_V
The short circuit current/temperature coefficient	K_I
The maximum experimental peak output power	P_{max}

Using theses information, we can present the I-V characteristic of a PV panel as following [17]:

$$I_{pv}=I_{ph}-I_0\left[exp\left(\frac{V_{pv}+R_{s,ar}I}{V_t a}\right)-1\right]-\frac{V_{pv}+R_{s,ar}I_{pv}}{R_{p,ar}} \quad (1)$$

$$I_{ph}=(I_{ph,n}+K_I(T-T_n))\frac{G}{G_n} \quad (2)$$

$$I_0=\frac{I_{sc,n}+K_I(T-T_n)}{exp\left(\frac{V_{oc,n}+K_V(T-T_n)}{V_t a}\right)-1} \quad (3)$$

where q is the electron charge, k is the Boltzmann constant, and a is the diode ideality constant. T and T_n are respectively, the actual and nominal temperatures of the p–n junction. $V_t = N_s kT/q$ is the thermal voltage of the array. I_{ph} and I_0 are respectively, the PV and saturation currents of the panel. $I_{ph,n}$ is the light-generated current at the nominal condition (T_n=25°C & G_n=1000 W/m^2). G is the irradiation on the device surface, $R_{s,ar}$ is the equivalent series resistance of the module and $R_{p,ar}$ is the equivalent parallel resistance while:

$$R_{s,ar}=\frac{N_s}{N_p}R_{s,cell}\,,\ R_{p,ar}=\frac{N_s}{N_p}R_{p,cell}$$

In the rest of this study a 26 Solarex MSX-60 photovoltaic module are considered to generate 1,5 KWc (Kilo Watt Peak). Each module consists of 36 polycrystalline silicon solar cells electrically configured in series with generated maximum power of 60W. 13 panels are assembled in series to generate a 200v−300v voltage range in a MPP operation under different climate changes. The characteristics of the considered MSX-60 are described in Appendix A. Figure 3a shows the Power/Voltage (P/V) curve of the considered module to different values of solar irradiance at the same value of temperature (25°C). However, Figure 3b describes the characteristic of the P/V curve of the same module to different value of temperature at the same value of radiation.

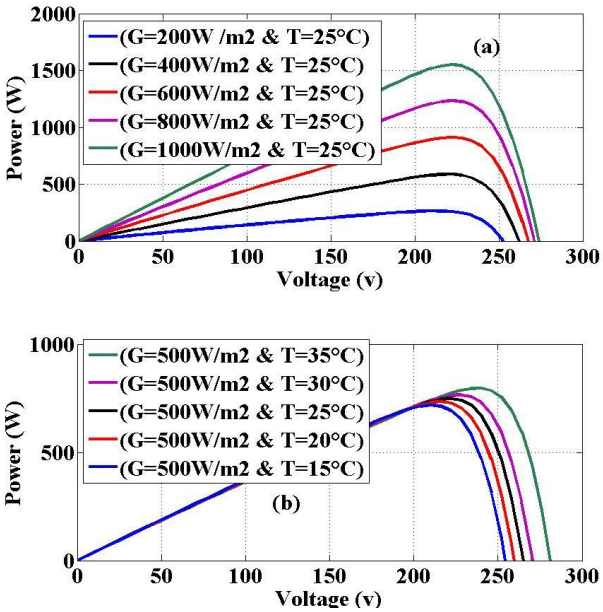

Figure 3: Power/Voltage curve of the considered PV module.

2.2. DC-DC boost converter & DC bus

DC-DC boost converters, frequently used in PV applications, are working as an impedance adapter to extract the maximum power from the PVG. A boost converter is a power converter with a DC output voltage higher than its voltage DC input (Figure 4).

Modelling booster chopper is obtained by the application of fundamental laws for the functioning of the system and can be expressed using the system of equations (4).

$$\begin{cases} \frac{dV_{pv}}{dt}=\frac{1}{C_1}(I_{pv}-I_{Lc}) \\ \frac{dI_{Lc}}{dt}=\frac{1}{L_c}(V_{pv}-V_{c_2}(1-D)) \\ \frac{dV_{dc}}{dt}=\frac{1}{C_2}(I_{Lc}(1-D)-I_{VSI}) \end{cases} \quad (4)$$

where I_{Lc} is the current across the inductor L_c, V_{dc} is the voltage in the capacitor C_2, D is the duty ratio of the PWM signal to control the switching MOSFET T_{Mos}. The characteristics of the electric components are described in Appendix A.

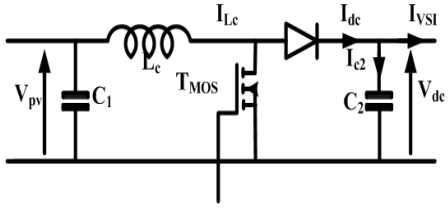

Figure 4: Boost DC-DC converter.

2.3. DC/AC inverter

In order to supply the IM, a power DC/AC (inverter) is used. This converter is composed by a three legs, each one is formed of two IGBTs and two diodes in anti-parallel. Each

transistor-diode assembly can be considered as an ideal switch (Figure 5).

To analyze the dynamic behaviour of the end to end system, it is convenient to adopt a global continuous model. Thus, it is necessary to develop an equivalent continuous model of the power converter using the Park transformation [18,19]. The output voltages of the DC/AC inverter are relative to the value of the DC bus voltage V_{dc} and the reference voltages (v^*_{sd}, v^*_{sq}) deduced from the Park transformation such that:

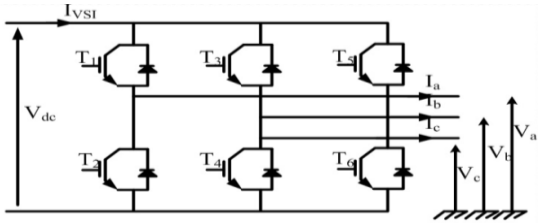

Figure 5: DC-AC inverter.

$$\begin{cases} v_{sd} = v^*_{sd}\dfrac{V_{dc}}{2} \\ v_{sq} = v^*_{sq}\dfrac{V_{dc}}{2} \end{cases} \quad (5)$$

The current modulated by the AC/DC inverter could be expressed as follow [12]:

$$I_{VSI} = v^*_{sd} i_{sd} + v^*_{sq} i_{sq} \quad (6)$$

where (i_{sd}, i_{sq}) are respectively the direct and the quadrature components of the currents at the inverter output in a synchronous rotating frame.

2.4. MPPT algorithm

The efficiency of stand-alone photovoltaic (PV) pumping systems can be significantly increased by employing a MPPT technique to optimize the delivered power regardless to variations in irradiation and temperature. Many techniques have been employed as constant voltage, INC, P&O algorithm etc. In this paper, a direct duty cycle P&O algorithm is employed due to its simplicity and its adequacy with non linear characteristic of the PVG [20].

2.5. Dynamic description of induction motor

The IM can be presented in a general d-q reference frame by the following model:

$$\begin{cases} \dot{i}_{sd} = -\gamma i_{sd} + \omega_a i_{sq} + \dfrac{K_S}{\tau_r}\Psi_{rd} + K_S n_p \omega_m \Psi_{rq} + \dfrac{1}{\sigma L_S} v_{sd} \\ \dot{i}_{sq} = -\omega_a i_{sd} - \gamma i_{sq} - K_S n_p \omega_m \Psi_{rd} + \dfrac{K_S}{\tau_r}\Psi_{rq} + \dfrac{1}{\sigma L_S} v_{sq} \\ \dot{\Psi}_{rd} = \dfrac{M}{\tau_r} i_{sd} - \dfrac{1}{\tau_r}\Psi_{rd} + (\omega_a - n_p\omega_m)\Psi_{rq} \\ \dot{\Psi}_{rq} = \dfrac{M}{\tau_r} i_{sq} - (\omega_a - n_p\omega_m)\Psi_{rd} - \dfrac{1}{\tau_r}\Psi_{rq} \\ J\dot{\omega}_m + f\omega_m = (T_e - T_l) \end{cases} \quad (7)$$

where $\gamma = \dfrac{1}{\sigma\tau_S} + \dfrac{1-\sigma}{\sigma\tau_r}, \sigma = 1 - \dfrac{M^2}{L_S L_r}, K_S = \dfrac{M}{\sigma L_S L_r}, \tau_S = \dfrac{L_S}{R_S}, \tau_r = \dfrac{L_r}{R_r}, (i_{sd}, i_{sq})$ are stator currents, (Ψ_{rd}, Ψ_{rq}) are rotor flux, (v_{sd}, v_{sq}) are stator voltages, R_S is the stator resistance, R_r is the rotor resistance, L_S is the stator self-inductance, L_r is the rotor self-inductance, M is the mutual inductance, σ is the leakage coefficient, ω_m is the motor angular velocity, ω_a is the angular velocity of the dq reference frame, ω_S is the synchronous angular velocity, f is the friction constant, J is the moment of inertia and n_p is the number of poles pairs. T_e and T_l are respectively, the magnetic torque and the load torque. The parameters of 1.5KW IM are described in the Appendix A.

2.6. Sensorless IRFOC strategy

1) <u>IRFOC strategy:</u> In the literature, many strategies of IM control were proposed for PV pumping systems, such that v/f (scalar control) or the vector control. Among these strategies previously cited, the vector control is considered as the most efficient. Hence, in this study, we will consider an IRFOC. This strategy is based on the control of the rotor flux Ψ_r, in a dq synchronous rotating reference frame ($\omega_a = \omega_S$), so that it is always aligned to the d-component Ψ_{rq} and equal to the reference flux Ψ^*_r. Then, the dynamic equation of the IM could be presented as follow:

$$v_{sd} = v_{sd1} + E_d \quad (8)$$

$$v_{sq} = v_{sq1} + E_q \quad (9)$$

such that:

$$\begin{aligned} v_{sd1} &= \sigma L_S\left[\dot{i}_{sd} + \gamma i_{sd}\right] // E_d = \sigma L_S\left[-\omega_S i_{sq} - \frac{K_S}{\tau_r}\Psi_{rd}\right] \\ v_{sq1} &= \sigma L_S\left[\dot{i}_{sq} + \gamma i_{sq}\right] // E_q = \sigma L_S\left[\omega_S i_{sd} + K_S\omega_S\Psi_{rd}\right] \end{aligned} \quad (10)$$

It can be seen that the d-axis and q-axis voltage equations are coupled by the terms E_d and E_q. These terms are considered as disturbances and are cancelled by using a decoupling method that utilizes nonlinear feedback of the coupling voltages.

We refer to Bahloul et al. [21] to design the IRFOC controller's gain (Figure 6). K_{iis} and K_{pis} are respectively the integral and the proportional gains of the currents controller. However, $K_{i\omega}$ and $K_{p\omega}$ denote the gains of the speed controller. The closed loop transfer functions are:

$$\frac{i_s}{i_s^*} = \frac{K_{iis}K_{pis}}{p^2 + \left(\dfrac{K_{pis} + \sigma L_S\gamma}{\sigma L_S}\right)p + \left(\dfrac{K_{iis}K_{pis}}{\sigma L_S}\right)} \quad (11)$$

$$\frac{\omega_m}{\omega_m^*} = \frac{K_{i\omega}K_{p\omega}}{Jp^2 + \left(f + K_{p\omega}\right)p + K_{i\omega}K_{p\omega}} \quad (12)$$

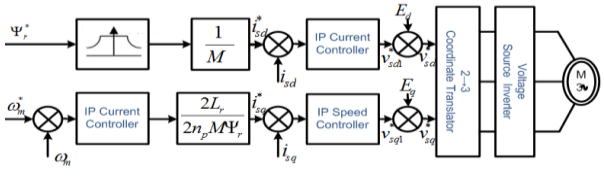

Figure 6: IRFOC structure.

2) Rotor speed estimation: It is worth to note that the IRFOC control of the IM requires rotor shaft speed information. Unfortunately, the use of speed sensors is so expensive relatively to the community concerned by such PV pumping application. In addition, it requires a periodic maintenance and it has an undesirable influence on the system reliability. Hence, a speed sensorless control has to be mandatory taken in consideration. Several speed estimation schemes, based on the IM model, were developed in the last decades [12,22,23]. We can distinguish the open loop methods and the closed loop one. In spite of the fact that the open loop speed estimation schemes are simpler than the closed loop one, they still suffering from a high sensitivity to the variation of the IM parameters [22]. Therefore the closed loop methods seem to be a preferable choice. In [12], a comparison study between a speed estimation algorithm based on Model Reference Adaptive System (MRAS), Reduced Adaptive Observer (RAO) and a Full Order Adaptive Observer (FOAO) was carried out. The authors consider, during tests, a direct FOC strategy to control the IM under a field weakening operation. On the basis of results presented in previous paper, we propose in this study to integrate an FOAO on the global system of control.

We recall hereunder the structure of the observer and the results presented in Kubota et al. [23] to estimate rotor speed $\hat{\omega}_m$. We note that this observer is synthesized on the basis of an IM model described in a stationary (α, β) reference frame $(\omega_a=0)$.

$$\begin{cases} \dot{\hat{x}}(t)=A(\hat{\omega}_m)\hat{x}(t)+Bu(t)+L\big(y(t)-\hat{y}(t)\big) \\ \hat{y}(t)=C\hat{x}(t) \end{cases} \tag{13}$$

such that:

$$L^T=\begin{bmatrix} L_1 & L_2 & L_3 & L_4 \\ -L_2 & L_1 & -L_4 & L_3 \end{bmatrix} \tag{14}$$

$$\hat{\omega}_m=K_P(e_{s\alpha}\hat{\Psi}_{r\beta}-e_{s\beta}\Psi_{r\alpha})+K_I\int(e_{s\alpha}\hat{\Psi}_{r\beta}-e_{s\beta}\hat{\Psi}_{r\alpha}) \tag{15}$$

$e_{s\alpha}=i_{s\alpha}-\hat{i}_{s\alpha}$, $e_{s\beta}=i_{s\beta}-\hat{i}_{s\beta}$. K_p and K_i are arbitrary positive gains. $x(t)=\begin{bmatrix} i_{s\alpha} & i_{s\beta} & \Psi_{r\alpha} & \Psi_{r\beta} \end{bmatrix}^T$ is the state vector, $y(t)=\begin{bmatrix} i_{s\alpha} & i_{s\beta} \end{bmatrix}^T$ present the output vector, $u(t)=\begin{bmatrix} v_{s\alpha} & v_{s\beta} \end{bmatrix}^T$ is the input vector, $\hat{x}(t)$ denotes the estimated state vector, $\hat{y}(t)$ is the observer outputs and L is the observer gain.

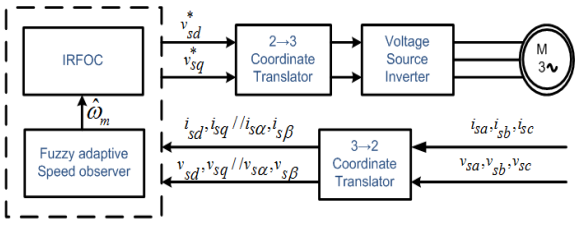

Figure 7: Block diagram of sensorless IRFOC of induction motor drive system.

2.7. Centrifugal pump model

The centrifugal pumps are widely employed for photovoltaic pumping applications. Indeed, they do not require a large torque at the start-up, so that they can be easily started by solar panels, even in low sunlight. Furthermore, they are too suitable for pumping water heavily laden with particles.

The flow-head characteristic of a centrifugal pump can be approximated by quadratic form using Pfleider–Peterman model [24], in which the rotor speed ω_m is a parameter:

$$H=n_0\omega_m^2+n_1\omega_m Q+n_2Q^2 \tag{16}$$

n_0, n_1, n_2 are the geometric parameters characterizing the pump.

The Q-H characteristic of the pipe network can be expressed by [25,26]:

$$H=Hg+\psi Q^2 \tag{17}$$

ψ is a constant which depends on conduit diameter and on all frictional losses of the pipe network.

The hydraulic power output of the pump and its efficiency can be expressed by the following equations:

$$P_h=\rho gQH$$

where ρ is the water density and g is the gravitational constant.

The volume of pumped water (m^3) during the operation system is then computed by: $V=Q\Delta T$ where ΔT is the pumping period.

A load torque proportional to the square of ω_m is generally considered to characterize the load applied by the pump on the rotor shaft of the IM [27] such that:

$$T_l=k_1\omega_m^2 \tag{18}$$

2.8. FLC controller

In the literature, several control strategies were adopted to control the pumping system and to improve the efficiency of the IM. Due to the nonlinear nature of the problem, the conventional PI controller could not achieve the desired performances. To deal with such problem, the Fuzzy Logic (FL) presents one of the most suitable techniques to deal with complex, nonlinear and uncertain problem. This strategy is widely used to control IM, PV or PV pumping system [25,27,28,29].

In this study a FLC is considered. The main aims of this controller could be described in twofold point.

1) To ensure a constant dc-link voltage via a balanced energy control between the DC-DC converter output, the dc-link capacitor and the IM. Indeed, through a variable reference speed applied as an input to the sensorless IRFOC algorithm, the IM power is controlled.

2) To maximize the efficiency of the IM by a control of the reference flux level especially at low speed when the load torque generated by the centrifugal is small.

The proposed FLC includes two input variables (I_{VSI} and V_{dc}) and two output variables ($\omega_m^{\star}$ and $\Psi_{rd}^{\star}$).

These variables are converted using fuzzification into linguistic fuzzy sets employing fuzzy membership function. Figure 8 shows the membership functions ($\mu_{Vdc}, \mu_{I_{VSI}}, \mu_{\omega_m^{\star}}, \mu_{\Psi_{rd}^{\star}}$) of the input and output variables.

In case of V_{dc}, seven fuzzy partitions are composed and nominated $V_{dci}=(A1,A2,...,A7)$. These partitions cover the fuzzy domain $V_{dc}=[0v,1000v]$.

In case of I_{VSI} ten fuzzy partitions are composed and nominated $I_{VSIi}=(B1,B2,...,B10)$. These partitions cover the fuzzy domain $I_{VSI}=[0A,3A]$.

In case of $\omega_m^{\star}$, eleven fuzzy partitions are composed and nominated $\omega_{mi}^{\star}=(T1,T2,...,T12)$. These partitions cover the fuzzy domain $\omega_m^{\star}=[0rad/s,160rad/s]$.

In case of $\Psi_r^{\star}$, six fuzzy partitions are composed and nominated $\Psi_{rdi}^{\star}=(S1,S2...,S6)$. These partitions cover the fuzzy domain $\Psi_{rd}^{\star}=[0.5Web,\ 1.2Web]$.

The fuzzy compensators are described in table II. The centre of area inference mechanism is used to calculate the fuzzy output.

3. Results and discussion

In order to validate the proposed control technique and show its effectiveness, a simulation of the system described in the Figure 1 was carried out using Matlab/Simulink software. The parameters of the PVG, DC/DC inverter, DC-bus, IM and pump are described in Appendix A.

In a first step, we chose to make a comparison between two algorithms. In the first one, the speed reference FLC output and a fixed rotor reference flux (1.1 Web) will be considered for the IRFOC bloc. In the second algorithm, the sensorless IRFOC is supplied by the two FLC outputs. The purpose of this study is to show the influence of the FLC on both the dc- bus and the efficiency of the IM (η).

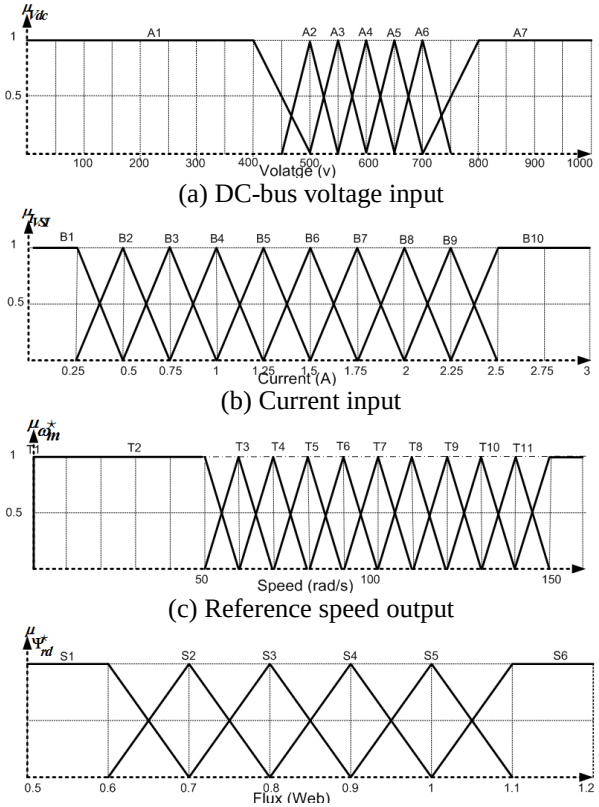

(a) DC-bus voltage input

(b) Current input

(c) Reference speed output

(d) Reference flux output

Figure 8: Membership functions of the FLC.

In the table III and the table IV, the main results are described. All values are taken in a steady state. From a V_{dc} control performances point of view, the two algorithms succeeded to maintain a V_{dc} value near to the reference one. The error is less than 5% of the reference.

Considering the IM efficiency, the second algorithm presents better performances for a low solar radiation. For both high and medium irradiation, the two algorithms seem to have the same performances. Figure 9 illustrates the two waveform of the IM efficiency of the two algorithms regarding the PVG output power. We note that the improvement of the IM efficiency is caused by the increase of the rotor speed on the shaft of the IM. On another hand, this improvement is accompanied by an energy saving and an increase in the quantity of the pumped water.

Table II: Rule base for the FLC.

V_{dc} / I_{VSI}	A1	A2	A3	A4	A5	A6	A7
B1	T1/S1	T1/S2	T1/S2	T2/S2	T2/S2	T3/S2	T4/S3
B2	T1/S1	T2/S3	T3/S3	T4/S4	T5/S4	T5/S4	T6/S5
B3	T1/S1	T3/S4	T4/S5	T5/S5	T6/S5	T6/S6	T8/S6
B4	T1/S1	T4/S6	T5/S6	T6/S6	T7/S6	T7/S6	T9/S6
B5	T1/S1	T5/S6	T5/S6	T7/S6	T7/S6	T8/S6	T10/S6
B6	T1/S1	T5/S6	T6/S6	T7/S6	T8/S6	T9/S6	T11/S6
B7	T1/S1	T6/S6	T7/S6	T8/S6	T9/S6	T10/S6	T11/S6
B8	T1/S1	T6/S6	T7/S6	T8/S6	T10/S6	T10/S6	T11/S6
B9	T1/S1	T7/S6	T7/S6	T9/S6	T10/S6	T11/S6	T11/S6
B10	T1/S1	T8/S6	T9/S6	T9/S6	T11/S6	T11/S6	T11/S6

Table III: Main results of the proposed system under different irradiation conditions without efficiency consideration (25°C).

G (W/m^2)	Vdc (v)	ω_r^* (rad/s-^{1})	Ψ_r^* (Web)	η %	Q (m^3/h)
100	595.83	49.44	1.1	56.18	8.39
200	599.76	73.80	1.1	73.61	12.52
300	591.61	87.26	1.1	77.83	14.80
400	596.63	98.32	1.1	79.50	16.67
500	594.25	106.42	1.1	80.35	18.05
600	606.14	113.79	1.1	80.77	19.30
700	600.28	120.22	1.1	80.99	20.39
800	611.43	126.00	1.1	81.07	21.37
900	601.33	131.19	1.1	81.10	22.25
1000	609.66	135.97	1.1	81.07	23.06

Table IV: Main results of the proposed system under different irradiation conditions with efficiency consideration (25°C).

G (W/m^2)	Vdc (v)	ω_r^* (rad/s-^{1})	Ψ_r^* (Web)	η %	Q (m^3/h)
100	597.34	52.47	0.7	67.15	8.90
200	599.82	73.90	0.85	73.69	12.53
300	597.20	86.84	0.97	77.45	14.73
400	596.80	97.82	1.12	79.63	16.59
500	594.41	106.50	1.12	80.53	18.06
600	606.37	113.90	1.12	80.99	19.32
700	600.44	120.34	1.12	81.24	20.41
800	611.78	126.13	1.12	81.33	21.39
900	601.55	1315.3	1.12	81.34	22.28
1000	610.02	136.13	1.12	81.39	23.09

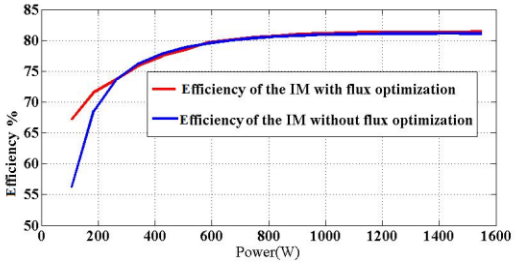

Figure 9: IM efficiency with and without flux optimization.

Now that we did a comparison between the two algorithms, we will deeply investigate in the second step, the dynamic performances using the second algorithm under different changes in solar radiation.

The solar irradiation level starts from 100 W /m^2, then increases to 550 W /m^2, after that increases to 1000 W /m^2, then decreases to 600 W /m^2 and reach finally the value of 200 W /m2. Each change takes 2s to move from the initial value to the final one, while the temperature is set to the value 25°C (Figure 10). The initial value of the dc-bus voltage, the PVG output and the duty cycle are considered such that V_{dc}=450v, V_{pv}=225v and D=0.5. The PVG power output is described in figure 11. Both, the PVG voltage output and the dc_bus voltage are shown in Figure 12. The current waveforms of the PVG output and the DC/DC inverter are described in Figure 13. The rotor speed reference (FLC output), the estimated rotor speed and the real rotor speed signals are presented in the Figure 14. The Figure 15 depicts the variation of the reference rotor flux (FLC output), the real d-component of the rotor flux as well as the estimated one. The real and the estimated q- axis components of the rotor flux are presented in Figure 16. The evolution of the duty cycle D is shown in Figure 17.

The analysis of the obtained results shows that the system presents a transient state following the start-up which disappears when the V_{dc} is quite near the reference. In addition a transient state is also presented following any changes on the solar radiation. However, its impacts on the dynamic performances of the system are minor. Indeed, V_{dc} is maintained near to the reference, the d-axis rotor flux follows the reference signal and the q-axis rotor flux is quite near to zero.

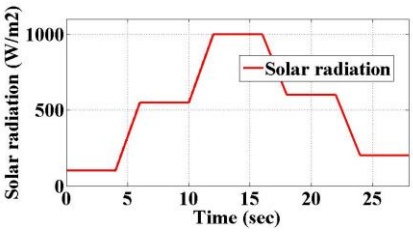

Figure 10: Solar radiation profile.

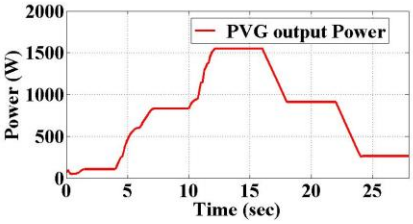

Figure 11: Output power of the PVG.

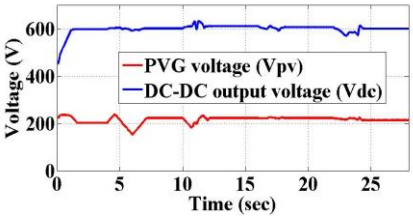

Figure 12: PVG voltage output (V_{pv}) & DC/DC voltage output (V_{dc}).

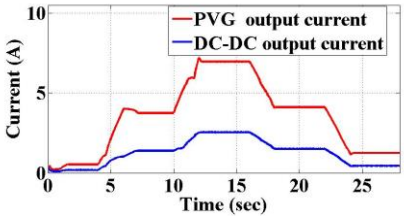

Figure 13: PVG current output (i_{pv}) & DC/DC current output (I_{dc})

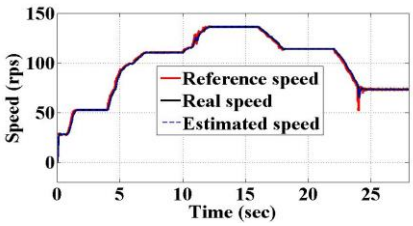

Figure 14: Reference speed & Real speed & Estimated speed of the IM

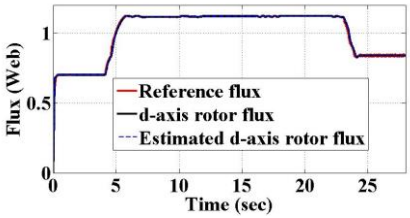

Figure 15: Reference Flux & d- axis Real Flux & d- axis Estimated Flux of the IM

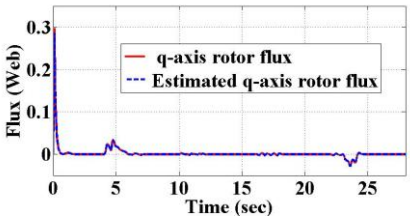

Figure 16: q- axis Real Flux & q- axis Estimated Flux of the IM

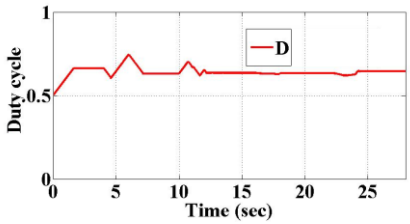

Figure 17: Duty cycle (DC/DC inverter control)

4. Conclusion

During this paper, we have focused on the development of a stand-alone autonomous PV pumping system. A batteryless configuration was proposed in order to overcome the problem caused by energy storage issues especially in remote areas. A robustness and economical consideration were taken into account, and which define the IM as the preferable solution for the pumping system. Three levels of energy consideration were taken into consideration. Indeed, a conventional MPPT P&O control and a sensorless IRFOC strategy were used and described. However, an intelligent control technique, on the basis of fuzzy logic, was proposed and investigated in order to optimize the flux in the IM. In addition, the same approach was used to control the dc-bus voltage. The performances of the system were proven through simulation and demonstrated the potential of the proposed method.

Appendix A

$V_{oc,n}=21.1v$	$K_V=-0.08$	$J=0.0049Kg.m^2$
$R_r=4.2\Omega$	$K_1=0.0005$	$n_s=36$
$R_s=5.72\Omega$	$M=0.4402H$	$L_s=0.462H$
$Q=26.64m^3/h$	$I_{mp}=3.5A$	$C_1=2010^{-6}F$
$H_g=7.4m$	$P_{max}=60W$	$C_2=35010^{-6}F$
$\omega_{mn}=1500tr/s$	$L_r=0.462H$	$f=0.003N.m.s.rd^{-1}$
$L_c=0.510^{-3}H$	$V_{mp}=17.1v$	$n_p=2$
$K_I=0.065$	$I_{sc,n}=3.8A$	$H=14m$

Appendix B

$$L_1=-(k-1)(\gamma+\frac{1}{Tr}),\ L_2=(k-1)n_p\hat{\omega}_m,$$

$$L_3=(k^2-1)(\frac{-\gamma}{K_S}+\frac{M}{T_r})+\frac{(k-1)}{K_S}(\gamma+\frac{1}{Tr}),\ L_4=-\frac{(k-1)}{K_S}n_p\hat{\omega}_m$$

$$A(\hat{\omega}_m)=\begin{bmatrix} -\gamma & 0 & \frac{K_S}{\tau_r} & K_S n_p\hat{\omega}_m \\ 0 & -\gamma & -K_S n_p\hat{\omega}_m & \frac{K_S}{\tau_r} \\ \frac{M}{\tau_r} & 0 & -\frac{1}{\tau_r} & -n_p\hat{\omega}_m \\ 0 & \frac{M}{\tau_r} & n_p\hat{\omega}_m & -\frac{1}{\tau_r} \end{bmatrix}$$

$$B=\begin{bmatrix} \frac{1}{\sigma L_S} & 0 & 0 & 0 \\ 0 & \frac{1}{\sigma L_S} & 0 & 0 \end{bmatrix}^T \quad C=\begin{bmatrix} 1 & 0 & 0 & 0 \\ 0 & 1 & 0 & 0 \end{bmatrix}$$

References

[1] R. Parajuli, G. Pokharel, and P. Østergaard, "A comparison of diesel, biodiesel and solar pv-based water pumping systems in the context of rural nepal," *International Journal of Sustainable Energy*, vol. 33, no. 3, pp. 536–553, 2014.

[2] C. Gopal, M. Mohanraj, P. Chandramohan, and P. Chandrasekar, "Renewable energy source water pumping systems-a literature review," *Renewable and Sustainable Energy Reviews*, vol. 25, no. 0, pp. 351 – 370, 2013.

[3] M. Elgendy, B. Zahawi, and D. Atkinson, "Comparison of directly connected and constant voltage controlled photovoltaic pumping systems," *Sustainable Energy, IEEE Transactions on*, vol. 1, pp. 184–192, Oct 2010.

[4] A. Betka and A. Attali, "Optimization of a photovoltaic pumping system based on the optimal control theory," *Solar Energy*, vol. 84, no. 7, pp. 1273 –1283, 2010.

[5] P. Periasamy, N.K. Jain and I.P. Singh , "A review on development of photovoltaic water pumping system," *Renewable and Sustainable Energy Reviews*, vol. 43, no. 0, pp. 918-925, 2015.

[6] S. Boukhalfa, F. Bouchafaa, T. Aounallah, "Optimisation of a GPV by an Artificial Intelligence Technical," *International Journal of Renewable Energy Research*, vol. 2, no. 4, pp. 730-735 , 2012.

[7] N. Mazouz and A. Midoun, "Control of a dc/dc converter by fuzzy controller for a solar pumping system," *International Journalof Electrical Power and Energy Systems*, vol. 33, no. 10, pp. 1623 – 1630, 2011.

[8] S. Lalouni, D. Rekioua, T. Rekioua, and E. Matagne, "Fuzzy logic control of stand-alone photovoltaic system with battery storage," *Journal of Power Sources*, vol. 193, no. 2, pp. 899 – 907, 2009.

[9] M. Vitorino, M. Beltrao de Rossiter Correa, C. Jacobina, and A. Lima, "An effective induction motor control for photovoltaic pumping," *Industrial Electronics, IEEE Transactions on*, vol. 58, pp. 1162–1170, April 2011.

[10] M. Mimouni, M. Mansouri, B. Benghanem, and M. Annabi, "Vectorial command of an asynchronous motor fed by a photovoltaic generator," *Renewable Energy*, vol. 29, no. 3, pp. 433 – 442, 2004.
[11] A. Khiareddine, C. Ben Salah, and M. F. Mimouni, "New methodology of speed-control of photovoltaic pumping system," *Journal of Renewable and Sustainable Energy*, vol. 5, no. 5, pp. –, 2013.
[12] G. Boukettaya, L. Krichen, and A. Ouali, "A comparative study of three different sensorless vector control strategies for a flywheel energy storage system," *Energy*, vol. 35, no. 1, pp. 132 – 139, 2010.
[13] F. Parasiliti and P. Bertoldi, Energy Efficiency in Motor Driven Systems. Springer Berlin Heidelberg, 2003.
[14] S. Sallem, M. Chaabene, and M. Kamoun, "Energy management algorithm for an optimum control of a photovoltaic water pumping system," *Applied Energy*, vol. 86, no. 12, pp. 2671 – 2680, 2009.
[15] T. Corrêa, S. S. Isaac, and S. Rocha Silva, "Efficiency optimization in stand-alone photovoltaic pumping system," *Renewable Energy*, vol. 41, no. 0, pp. 220 – 226, 2012.
[16] J. Mapurunga Caracas, G. De Carvalho Farias, L. Moreira Teixeira, and L. de Souza Ribeiro, "Implementation of a high-efficiency, high-lifetime, and low-cost converter for an autonomous photovoltaic water pumping system," *Industry Applications, IEEE Transactions on*, vol. 50, pp. 631–641, Jan 2014.
[17] M. Villalva, J. Gazoli, and E. Filho, "Comprehensive approach to modeling and simulation of photovoltaic arrays," *Power Electronics, IEEE Transactions on*, vol. 24, pp. 1198–1208, May 2009.
[18] B. Robyns, Y. Pankow, L. Leclercq, and B. François, "Equivalent continuous dynamic model of renewable energy systems," in 7th *International Conference on Modelling and Simulation of Electric machines, Converters and Systems:Electrimacs* 2002, CD, 18-21 Aout 2002, Montreal, Canada, pp. 1–1, 2002.
[19] B. François and J. Hautier, "Commande d'un onduleur triphasè de tension par modulateur de largeur et de position d'impulsions*," Revue Internationale de Génie Electrique*, vol. 2, no. 3, pp. 359–387, 1999.
[20] M. Elgendy, B. Zahawi, and D. Atkinson, "Assessment of perturb and observe mppt algorithm implementation techniques for pv pumping applications," *Sustainable Energy*, IEEE Transactions on, vol. 3, pp. 21–33, Jan 2012.
[21] M. Bahloul, M. Souissi, M. Chaabane, and L. Chrifi-Alaoui, "Takagi sugeno fuzzy observer based direct rotor field oriented control of induction machine," *in Systems and Control (ICSC), 2013 3rd International Conference on*, pp. 419–426, Oct 2013.
[22] I. Alsofyani and N. Idris, "A review on sensorless techniques for sustainable reliablity and efficient variable frequency drives of induction motors," *Renewable and Sustainable Energy Reviews*, vol. 24, no. 0, pp. 111 – 121, 2013.
[23] H. Kubota, K. Matsuse, and T. Nakano, "Dsp-based speed adaptive flux observer of induction motor," *IEEE Transactions on Industry Applications*, vol. 29, pp. 344 –348, Mar./Apr. 1993.
[24] A. Betka and A. Moussi, "Optimized solar water pumping system based on an induction motor driving a centrifugal pump," *in Proceedings of the 4th WSEAS International Conference on Applications of Electrical Engineering*, AEE'05, pp. 305–313, 2005.
[25] K. Benlarbi, L. Mokrani, and M. Nait-Said, "A fuzzy global efficiency optimization of a photovoltaic water pumping system," *Solar Energy*, vol. 77, no. 2, pp. 203 – 216, 2004.
[26] T. Ahonen, J. Tamminen, J. Ahola, and J. Kestila, "Frequency-converter-based hybrid estimation method for the centrifugal pump operational state," *Industrial Electronics, IEEE Transactions on*, vol. 59, pp. 4803–4809, Dec 2012.
[27] B. Kumar, Y. K. Chauhan, and V. Shrivastava, "A comparative study of maximum power point tracking methods for a photovoltaic-based water pumping system," *International Journal of Sustainable Energy*, vol. 33, no. 4, pp. 797–810, 2014.
[28] R. Arulmurugan and N. Suthanthiravanitha, "Adaptive fuzzy logic control based optimal hopfield neural network of standalone photovoltaic system with battery storage," *Journal of Renewable and Sustainable Energy*, vol. 6, no. 3, pp. –, 2014.
[29] S.-M. Yang and F.-C. Lin, "Loss minimization control of vector controlled induction motor drives," *Journal of the Chinese Institute of Engineers*, vol. 26, no. 1, pp. 37–45, 2003.